Check for updates

Complete measurement of spatiotemporally complex multi-spatial-mode ultrashort pulses from multimode optical fibers using delay-scanned wavelength-multiplexed holography

PING ZHU,[1,2,3,*] RANA JAFARI,[2] TRAVIS JONES,[2] AND RICK TREBINO[2]

[1]National Laboratory on High Power Laser and Physics, Shanghai Institute of Optics and Fine Mechanics, Chinese Academy of Sciences, Shanghai 201800, China
[2]School of Physics, Georgia Institute of Technology, 837 State Street, Atlanta, Georgia 30332, USA
[3]University of the Chinese Academy of Sciences, Beijing 100049, China
*zhp1990@siom.ac.cn

Abstract: We introduce a simple delay-scanned complete spatiotemporal intensity-and-phase measurement technique based on wavelength-multiplexed holography to characterize long, complex pulses in space and time. We demonstrate it using pulses emerging from multi-mode fiber. This technique extends the temporal range and spectral resolution of the single-frame STRIPED FISH technique without using an otherwise-required expensive ultranarrow-bandpass filter. With this technique, we measured the complete intensity and phase of up to ten fiber modes from a multi-mode fiber (normalized frequency $V \approx 10$) over a ~3ps time range. Spatiotemporal complexities such as intermodal delay, modal dispersion, and material dispersion were also intuitively displayed by the retrieved results. Agreement between the reconstructed color movies and the monitored time-averaged spatial profiles confirms the validity to this delay-scanned STRIPED FISH method.

References and links

1. D. J. Richardson, J. Nilsson, and W. A. Clarkson, "High power fiber lasers: current status and future perspectives [Invited]," J. Opt. Soc. Am. B **27**(11), B63–B92 (2010).
2. A. Liem, D. Nickel, J. Limpert, H. Zellmer, U. Griebner, S. Unger, A. Tunnermann, and G. Korn, "High average power ultra-fast fiber chirped pulse amplification system," Appl. Phys. B-Lasers Opt. **71**(6), 889–891 (2000).
3. D. J. Richardson, J. M. Fini, and L. E. Nelson, "Space-division multiplexing in optical fibres," Nat. Photonics **7**(5), 354–362 (2013).
4. R. Ryf, S. Randel, A. H. Gnauck, C. Bolle, A. Sierra, S. Mumtaz, M. Esmaeelpour, E. C. Burrows, R.-J. Essiambre, P. J. Winzer, D. W. Peckham, A. H. McCurdy, and R. Lingle, "Mode-Division Multiplexing Over 96 km of Few-Mode Fiber Using Coherent 6 × 6 MIMO Processing," J. Lightwave Technol. **30**(4), 521–531 (2012).
5. L. G. Wright, D. N. Christodoulides, and F. W. Wise, "Controllable spatiotemporal nonlinear effects in multimode fibres," Nat. Photonics **9**(5), 306–310 (2015).
6. A. S. Kurkov, E. M. Sholokhov, and Y. E. Sadovnikova, "All-fiber supercontinuum source in the range of 1550-2400 nm based on telecommunication multimode fiber," Laser Phys. Lett. **8**(8), 598–600 (2011).
7. F. Poletti and P. Horak, "Description of ultrashort pulse propagation in multimode optical fibers," J. Opt. Soc. Am. B **25**(10), 1645–1654 (2008).
8. J. W. Nicholson, A. D. Yablon, S. Ramachandran, and S. Ghalmi, "Spatially and spectrally resolved imaging of modal content in large-mode-area fibers," Opt. Express **16**(10), 7233–7243 (2008).
9. D. R. Gray, M. N. Petrovich, S. R. Sandoghchi, N. V. Wheeler, N. K. Baddela, G. T. Jasion, T. Bradley, D. J. Richardson, and F. Poletti, "Real-Time Modal Analysis via Wavelength-Swept Spatial and Spectral (S-2) Imaging," IEEE Photonics Technol. Lett. **28**, 1034–1037 (2016).
10. D. N. Schimpf, R. A. Barankov, and S. Ramachandran, "Cross-correlated (C2) imaging of fiber and waveguide modes," Opt. Express **19**(14), 13008–13019 (2011).
11. Z. Zhu, L. G. Wright, D. N. Christodoulides, and F. W. Wise, "Observation of multimode solitons in few-mode fiber," Opt. Lett. **41**(20), 4819–4822 (2016).

12. S. Akturk, M. Kimmel, P. O'Shea, and R. Trebino, "Measuring pulse-front tilt in ultrashort pulses using GRENOUILLE," Opt. Express **11**(5), 491–501 (2003).
13. P. Bowlan, U. Fuchs, R. Trebino, and U. D. Zeitner, "Measuring the spatiotemporal electric field of tightly focused ultrashort pulses with sub-micron spatial resolution," Opt. Express **16**(18), 13663–13675 (2008).
14. F. Bonaretti, D. Faccio, M. Clerici, J. Biegert, and P. Di Trapani, "Spatiotemporal Amplitude and Phase Retrieval of Bessel-X pulses using a Hartmann-Shack Sensor," Opt. Express **17**(12), 9804–9809 (2009).
15. E. Rubino, D. Faccio, L. Tartara, P. K. Bates, O. Chalus, M. Clerici, F. Bonaretti, J. Biegert, and P. Di Trapani, "Spatiotemporal amplitude and phase retrieval of space-time coupled ultrashort pulses using the Shackled-FROG technique," Opt. Lett. **34**(24), 3854–3856 (2009).
16. Z. Guang, M. Rhodes, and R. Trebino, "Measuring spatiotemporal intensity-and-phase complexity of multimode fiber output pulses," in Proceedings **9740**, Frontiers in Ultrafast Optics: Biomedical, Scientific, and Industrial Applications XVI; 97400G (2016).
17. D. Gloge, "Weakly Guiding Fibers," Appl. Opt. **10**(10), 2252–2258 (1971).
18. D. Gloge, "Dispersion in Weakly Guiding Fibers," Appl. Opt. **10**(11), 2442–2445 (1971).
19. P. O'Shea, M. Kimmel, X. Gu, and R. Trebino, "Highly simplified device for ultrashort-pulse measurement," Opt. Lett. **26**(12), 932–934 (2001).
20. Z. Guang, M. Rhodes, M. Davis, and R. Trebino, "Complete characterization of a spatiotemporally complex pulse by an improved single-frame pulse-measurement technique," J. Opt. Soc. Am. B **31**(11), 2736 (2014).
21. J. Cohen, P. Bowlan, V. Chauhan, and R. Trebino, "Measuring temporally complex ultrashort pulses using multiple-delay crossed-beam spectral interferometry," Opt. Express **18**(7), 6583–6597 (2010).
22. J. Cohen, P. Bowlan, V. Chauhan, P. Vaughan, and R. Trebino, "Measuring extremely complex pulses with time-bandwidth products exceeding 65,000 using multiple-delay crossed-beam spectral interferometry," Opt. Express **18**(24), 24451–24460 (2010).
23. M. Takeda, H. Ina, and S. Kobayashi, "Fourier-transform method of fringe-pattern analysis for computer-based topography and interferometry," J. Opt. Soc. Am. A **72**(1), 156–160 (1982).
24. R. P. Encyclopedia, "Multimode fibers," *https://www.rp-photonics.com/multimode_fibers.html*.
25. J. A. Buck, *Fundamentals of Optical Fibers* (John Wiley & Sons, 2004).
26. S. Das, C. G. Englefield, and P. A. Goud, "Power loss, modal noise and distortion due to microbending of optical fibers," Appl. Opt. **24**(15), 2323–2334 (1985).
27. K. Kitayama and M. Ikeda, "Mode mixing effects in optical fibers caused by sheathing and multistranding: measurements," Appl. Opt. **17**(22), 3660–3664 (1978).

1. Introduction

Multi-mode fibers (MMFs) are anticipated to have many important applications. Due to their large mode area and large information transmission capacity, MMFs have been considered for such uses as in high powered fiber lasers [1, 2], space-division-multiplexing communication systems [3, 4], as well as other interesting nonlinear optical phenomena [5,6]. Recently, work has been done to demonstrate the complex spatiotemporal nature of the dynamics of ultrafast pulses as they propagate through MMF [5, 7]. More specifically, it has been shown that these dynamics are inherently coupled in space and time. These spatiotemporal couplings can give rise to certain pulse distortions within the fiber, such as intermodal delay and modal dispersion, which can complicate the use of an ultrashort pulse for its intended application. Thus, as we continue to seek ways to incorporate MMFs into new technology, it becomes increasingly apparent that we should also seek to fully understand the pulses emerging from them. Simply put, to better understand the potential of MMFs for these applications, a direct, complete, and reliable knowledge of the complex spatiotemporally-coupled optical field inside the MMF is essential.

A number of techniques have been proposed to meet the need for a better understanding of the pulses emerging from MMF, but many of the techniques proposed fall short of obtaining the pulse's information completely and simultaneously in space and time. Among them are techniques such as spatially and spectrally resolved (S^2) imaging [8, 9], wavelength sweeping using a fast camera [9], and cross-correlation (C^2) imaging [10]. The notable feature of these techniques is their ability to conduct modal analysis and sufficiently determine the modal content of the pulses emerging from MMFs. These techniques, however, monitor the pulse either temporally or spatially only, while integrating over the other coordinate. As a result, these techniques are unable to capture possible spatiotemporally coupled distortions. For this reason, these techniques cannot be used to obtain a complete spatiotemporal characterization of a pulse emerging from a MMF. Another proposed technique that examines

spatiotemporally complex solitons in few-mode fiber uses a spatial camera, spectrometer, and intensity autocorrelation to obtain pulse information in the spatial, spectral, and temporal domains separately [11]. This technique, much like those previously mentioned, also lacks the ability to detect spatiotemporally coupled effects and therefore is also unsuitable for a complete MMF pulse measurement. And while other spatiotemporal approaches have also been proposed, including spatially extended temporal techniques [12, 13] and spectrally or temporally extended spatial techniques [14, 15], unfortunately none of them can directly obtain the spatiotemporal information of pulses from MMFs simultaneously, or even fully, and thus cannot be used for modal analysis.

Recently, a promising pulse measurement technique called Spatially and Temporally Resolved Intensity and Phase Evaluation Device: Full Information from a Single Hologram (STRIPED FISH) has been shown to successfully measure the potentially complex, real-time spatiotemporal intensity and phase of MMF output pulses on a single camera frame. This simple device spatiotemporally resolves the pulse structures: spatially on a micron scale and temporally on a femtosecond scale [16] *simultaneously*. To our knowledge, STRIPED FISH is the only device ever proposed that is capable of full spatiotemporal-pulse characterization and hence complete modal analysis.

Most recently, single-frame STRIPED FISH has demonstrated its ability to completely characterize few-mode pulses as they emerge from MMF. Limited by its few hundred femtosecond temporal measurement range, however, the technique was only able to measure the first four lowest-order modes closely spaced in time. Due to the potentially large intermodal delay, modal dispersion, and material dispersion present in MMF [17, 18], pulses can become significantly longer and even more complex after propagation through a segment of MMF. And while the material dispersion, which temporally stretches different frequency components along the fiber, could be easily compensated for by introducing additional negative dispersion to the pulse [16], the intermodal delay and modal dispersion inevitably spread different modes with different velocities over a potentially much longer time range. The current temporal measurement range of a typical single-frame STRIPED FISH, as determined by its critical component, the bandpass filter [19, 20], is insufficient for measuring the longer pulses that propagate over longer segments of MMF and contain a larger number of modes.

Consequently, here, we introduce a technique that extends the temporal range of STRIPED FISH enabling it to completely measure the spatiotemporal intensity and phase of longer, more complex pulses emitted from MMFs comprising more fiber modes. Instead of using a single-frame STRIPED FISH trace, which would require an extremely expensive (and still limited) ultranarrow bandpass filter, we use multiple delays, capturing STRIPED FISH traces for all delayed slices of the long pulse. The final spatiotemporal pulse field is reconstructed by concatenating the retrieved intensity and phase of these delayed slices in the time domain. We call it delay-scanned STRIPED FISH. This technique retains its simple apparatus and also remains easy to perform, involving scanning in only one dimension. Along with its extended temporal range, the resulting spectral resolution is also improved (to the reciprocal of the delay range), and, unlike the previous single-frame STRIPED FISH technique, is now independent of the filter's bandpass width. To confirm the improved capability offered by this technique, we experimentally generated long complex pulses from MMF, comprising more than ten fiber modes. We then spatiotemporally measured them over a ~3ps time range, ultimately presenting the complete intensity and phase information of the pulses intuitively in the format of color movies. While the temporal measurement range presented here demonstrates roughly a factor of 10 improvement over the single shot device, this delay-scanned STRIPED FISH technique can be applied to arbitrary pulse lengths provided that the requisite delay range can be achieved. Indeed, using a state-of-the-art narrowband filter and high-dynamic-range camera, the temporal range of delay-scanned

STRIPED FISH could be extended by a factor of >10,000. Our more modest implementation here should be considered a proof of this principle.

2. Extending STRIPED FISH to longer and more complex pulses

The single-frame STRIPED FISH apparatus is shown in Fig. 1(a). Its simple structure involves only a coarse two-dimensional diffractive optical element (DOE), an interference narrow bandpass filter (IBPF), imaging optics, and a camera. The unknown pulse to be measured, along with a spatially filtered and FROG-measured [19] reference pulse, propagate with a small vertical crossing angle through a slightly rotated DOE, simultaneously generating multiple pairs of beams that diverge at different angles both vertically and horizontally. Since the wavelength transmitted by the bandpass filter depends on the beam's incidence angle, the different beam pairs' incidence angles on the IBPF cause the transmitted wavelengths of the beam pairs to be different. These wavelength-filtered beam pairs, whose spectral widths are the IBPF's bandpass width, then overlap at the imaging camera, generating an array of quasi-monochromatic holograms, each at a different wavelength. Several optics, such as photography lenses and an apodizing neutral density filter (ANDF), can also be used to control optical aberrations (mostly barrel distortion) and balance the intensity of each hologram [20]. A simulated typical STRIPED FISH trace for a simple flat-phase Gaussian pulse is shown in Fig. 1(b). The different colors (false colors) of the holograms represent the locations of different wavelengths while all the spatiotemporal information is contained within the fringes of the multiple holograms, all of which are simultaneously recorded on one camera frame.
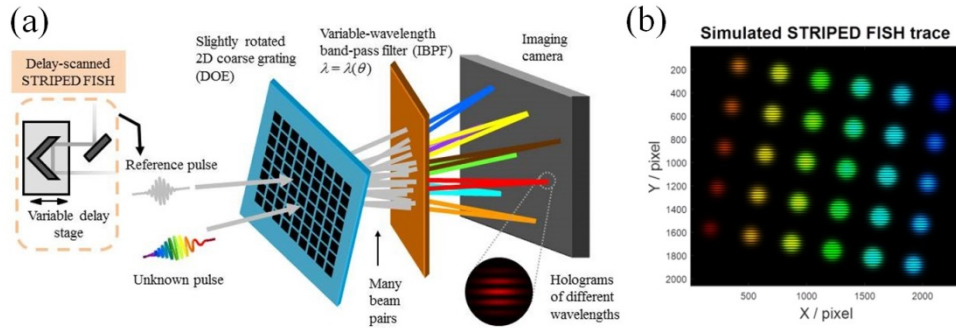
Fig. 1. (a) Excluding the elements in the dashed orange rectangle, this is a schematic of a single-frame STRIPED FISH apparatus. By incorporating the variable delay stage (depicted in the dashed rectangle) into a single-frame STRIPED FISH setup, this becomes a schematic for delay-scanned STRIPED FISH. (b) A simulated STRIPED FISH trace for a simple flat-phase Gaussian pulse. False colors are used to indicate the different wavelengths of the holograms. In this work, we extend single-frame STRIPED FISH to multiple frames, one for each delay over a potentially large range of delays.

Since the interference fringes are necessary for retrieving the unknown pulse, STRIPED FISH requires spectral and temporal overlap of the reference and unknown pulses. By the uncertainty principle, after wavelength-filtering by the IBPF, the essentially monochromatic pulses broaden by the reciprocal of the bandwidth of the bandpass filter. The unknown pulses that could be measured can thus be no longer than the bandpass-filter-stretched reference pulse, which means the temporal range ΔT_{SF} of single-frame STRIPED FISH is limited by the bandpass filter's bandwidth:

$$\Delta T_{\text{SF}} = \frac{2\pi}{\delta\omega_{\text{filter}}} = \frac{\lambda_0{}^2}{c\,\delta\lambda_{\text{filter}}}. \tag{1}$$

To measure longer pulses, single-frame STRIPED FISH must be equipped with a much narrower bandpass filter, which can be both difficult to manufacture and expensive. Alternatively, if the pulse train is stable and the measurement can be made by averaging over one to two seconds, then scanning the delay and using a numerical time-concatenation technique can extend the measurable time-bandwidth product. This approach has been demonstrated in a previous version of spectral interferometry [21, 22] and can be used here to extend STRIPED FISH to a longer temporal measurement range and higher spectral resolution in a simple and inexpensive way.

As a result, instead of acquiring a single frame with many high-spectral-resolution holograms, multiple frames of fewer lower-spectral-resolution STRIPED FISH traces are acquired at different delays over a long delay scanning range ΔT_{delay}. We then reconstruct the pulse from these multiple frames to yield the longer pulse in its entirety. Moreover, by extending the temporal range of the device in this way, the effective spectral resolution is also enhanced as seen from Eq. (2). This improvement to the spectral resolution better equips delay-scanned STRIPED FISH for more complex pulses.

$$\delta\lambda_{\text{eff}} = \frac{\lambda_0^2}{c\left(\Delta T_{\text{delay}} + \Delta T_{\text{SF}}\right)} = \frac{\Delta T_{\text{SF}}}{\Delta T_{\text{delay}} + \Delta T_{\text{SF}}}\delta\lambda_{\text{SF}} \approx \frac{\Delta T_{\text{SF}}}{\Delta T_{\text{delay}}}\delta\lambda_{\text{SF}} \tag{2}$$

The last expression holds when the delay range ΔT_{delay} is much longer that the inverse filter bandwidth ΔT_{SF}.

In the next section, we will describe the delay-scanned STRIPED FISH retrieval algorithm and pulse visualization method. An experiment in which we measure ~3ps output pulses with structures from more than ten fiber modes from a MMF will be described in section 4. In section 5, we will discuss the measured and reconstructed results. And finally, in section 6, we will describe delay-scanned STRIPED FISH's limitations.

3. Retrieval algorithm and pulse visualization

On a given frame, delay-scanned STRIPED FISH yields multiple holograms, I_{holo}, of different wavelengths, ω_i, at different delays, τ_k. If α is the small vertical crossing angle between the reference pulse E_{ref} and the unknown pulse E_{unk}, the detected intensity is given by:

$$\begin{aligned}
I_{\text{holo}}\left(x, y, \omega_i; \tau_k\right) = {} & I_{\text{ref}}\left(x, y, \omega_i\right) + I_{\text{unk}}\left(x, y, \omega_i\right) \\
& + E_{\text{ref}}\left(x, y, \omega_i; \tau_k\right)E_{\text{unk}}^*\left(x, y, \omega_i; \tau_k\right)\exp\left(ik_i y \sin\alpha\right) \\
& + E_{\text{ref}}^*\left(x, y, \omega_i; \tau_k\right)E_{\text{unk}}\left(x, y, \omega_i; \tau_k\right)\exp\left(-ik_i y \sin\alpha\right).
\end{aligned} \tag{3}$$

The first two terms contribute to a constant background during the delay scanning. The third term and its conjugate contain modulation terms, $\exp(\pm ik_i y \sin\alpha)$, which form the informative fringes shown in Fig. 1(b).

3.1 Field reconstruction for every delayed slice

To retrieve the intensity and phase of every delayed slice of the unknown pulse from the measured holograms, a spatial Fourier filtering algorithm [23] is used to isolate the background and fringe terms and to extract the product of the reference and unknown spatio-spectral complex fields at every delay, $E_{\text{ref}}(x,y,\omega_i;\tau_k)E^*_{\text{unk}}(x,y,\omega_i;\tau_k)$, whose argument is the spectral phase difference between the reference pulse and the unknown delayed slice:

$$\Delta\varphi\left(x, y, \omega_i; \tau_k\right) = \text{Arg}\left[E_{\text{ref}}\left(x, y, \omega_i; \tau_k\right)E_{\text{unk}}^*\left(x, y, \omega_i; \tau_k\right)\right]. \tag{4}$$

With knowledge of the reference pulse's intensity and phase, the spatio-spectral field of a delayed slice can be reconstructed using:

$$E_{\mathrm{slice}}\left(x,y,\omega_i;\tau_k\right) = \sqrt{\frac{\left|E_{\mathrm{ref}}\left(x,y,\omega_i;\tau_k\right)E_{\mathrm{unk}}^{*}\left(x,y,\omega_i;\tau_k\right)\right|}{\left|E_{\mathrm{ref}}\left(x,y,\omega_i\right)\right|^2}}\exp\left[-i\varphi_{\mathrm{slice}}\left(x,y,\omega_i;\tau_k\right)\right], \quad (5)$$

$$\varphi_{\mathrm{slice}}\left(x,y,\omega_i;\tau_k\right) = \varphi_{\mathrm{ref}}\left(x,y,\omega_i\right) - \Delta\varphi\left(x,y,\omega_i;\tau_k\right).$$

After the bandpass filter, each slice's duration, within which the delayed reference pulse interferes with the unknown pulse, is ΔT_{SF} according to Eq. (1). Only the information located in this time window is valid; information outside of this region should be cropped out. Thus, the spatiotemporal field of every delayed slice can be easily gained by performing a time-spectrum Fourier transformation and temporal filtering, yielding:

$$E_{\mathrm{slice}}(x,y,t;\tau_k) = \begin{cases} F^{-1}\left\{E_{\mathrm{slice}}(x,y,t;\tau_k)\right\}, & \text{if } \tau_k - \dfrac{\Delta T_{\mathrm{SF}}}{2} < t < \tau_k + \dfrac{\Delta T_{\mathrm{SF}}}{2}; \\ 0, & \text{otherwise;} \end{cases} \quad (6)$$

$$= A_{\mathrm{slice}}(x,y,t;\tau_k)\exp\left[-i\varnothing_{\mathrm{slice}}(x,y,t;\tau_k)\right].$$

3.2 Concatenation of multiple delayed slices

A concatenation procedure, along with a temporal axis transformation and Gaussian-weighted averaging, can be performed on the multiple retrieved slice fields obtained from the previous section to completely spatiotemporally characterize the unknown pulse.

While the temporal axis of each time (local) slice is centered at τ_k, with a window of ΔT_{SF}, the entire unknown pulse's temporal (global) range is extended to $\Delta T_{\mathrm{delay}} + \Delta T_{\mathrm{SF}}$, centered at zero delay. Yet, because of the unchanged spectral detection range during the delay scanning, the temporal resolution of both temporal axes should remain the same based on the uncertainty principle. Based on the temporal range and resolution, a global temporal axis for the entire unknown pulse is determined for the concatenation.

A Gaussian-weighted averaging scheme [21] is then implemented to minimize the concatenation discontinuities caused by possible reference pulse instability and delay scanning noise—although the laser source and delay stage were usually stable. A Gaussian-weighted function, centered on τ_k with a half width, τ_{G}, at 1/e, is chosen for the τ_k delayed slice:

$$G_{weight}\left(t;x,y,\tau_k\right) = \exp\left[-\left(\frac{t-\tau_k}{\tau_{\mathrm{G}}}\right)^2\right]. \quad (7)$$

The selection of the width of this Gaussian function was not seen to affect the accuracy of the concatenation as long as it was less than ΔT_{SF}, but larger than or equal to the delay interval τ_{delay}. Since ΔT_{SF} is longer than τ_{delay}, there is some redundancy in the information obtained from the overlap between delayed slices. This redundancy should make for higher-quality retrieval. Meanwhile, the Gaussian-weighted averaging provides the information near the temporal center of each time slice with a stronger contribution, improving the accuracy of the concatenation results. The final concatenated spatiotemporal electric field of the entire unknown pulse can be derived as:

$$E_{\mathrm{unk}}\left(x,y,t\right) = \frac{\sum\limits_{k=1}^{N} G_{weight}\left(t;x,y,\tau_k\right) E_{\mathrm{slice}}\left(x,y,t;\tau_k\right)}{\sum\limits_{k=1}^{N} G_{weight}\left(t;x,y,\tau_k\right)}, \quad (8)$$

where N is the number of recorded frames.

3.3 Spatiotemporal pulse visualization

Once the complete spatiotemporal pulse field, $E_{unk}(x,y,t)$, is acquired, it is also important to display the three-dimensional intensity and phase in an intuitive way. Firstly, the spectrogram at every spatial position, $Sp(\omega,T;x,y)$, is computed for simulating how the human eye responds to color:

$$Sp(\omega,T;x,y) = \left| \int_{-\infty}^{\infty} E(t;x,y) g(t-T) \exp(-i\omega t) \, dt \right|^2 , \qquad (9)$$

where $g(t-T)$ is a numerically generated gate function at the variably delayed T, which has the width of a fraction of the pulse length. Then, the spectrogram is multiplied by the color response functions $R(\omega)/G(\omega)/B(\omega)$, and integrated into RGB color values, which, in this paper, are false-color Gaussian functions centered at red wavelength (~806 nm)/ green wavelength (~795 nm)/ blue wavelength (~785 nm):

$$R(T;x,y) = \int_{-\infty}^{\infty} Sp(\omega,T;x,y)R(\omega)\mathrm{d}\omega; \quad G(T;x,y) = \int_{-\infty}^{\infty} Sp(\omega,T;x,y)G(\omega)\mathrm{d}\omega;$$

$$(10)$$

$$B(T;x,y) = \int_{-\infty}^{\infty} Sp(\omega,T;x,y)B(\omega)\mathrm{d}\omega.$$

The appearance of a color represents the presence of the corresponding wavelength or frequency component(s) of the pulse; the pulse will look white when all components of the spectrum are present at the same point in space and time (see Appendix). In addition, the variation in the colors over time represents phase variations in the pulse such as dispersion and delay.

In this way, complex spatiotemporal pulses can be visualized as if we could "see" them with such high temporal resolution. Spatially in a two-dimensional movie frame and temporally between frames, the brightness gives the relative intensity and changes in color represent phase information of the spatiotemporal pulse field.

3.4 Modal decomposition analysis

If the fiber modes contained in the pulses are well separated in time, we can easily tell which mode is present at each time by directly observing the color movies. However, when multiple fiber modes overlap in time, modal decomposition should be used for analyzing the modal contents and modal weights based on linearly polarized (LP) fiber modes. These modes are orthogonal to each other and their expressions are:

$$E_{lmi} = A_{lmi} \begin{cases} J_l\left(\dfrac{u_{lm}r}{a}\right)\Phi_i, & r \le a; \\[2ex] \dfrac{J_l(u_{lm})}{K_l(w_{lm})} K_l\left(\dfrac{w_{lm}r}{a}\right)\Phi_i, & r \ge a; \end{cases} , \quad \Phi_i = \begin{cases} \cos(l\varphi), & i=e; \\ \sin(l\varphi), & i=o; \end{cases} \quad (11)$$

where a is the radius of fiber core; J and K are Bessel functions and modified Bessel functions, respectively, and A is the normalization constant. The values of parameters u and w, related by normalized frequency parameter V, also known as V number, are found by numerically solving the eigenvalue equation in the step index fiber [25].

$$\frac{J_{l-1}(u)}{J_l(u)} = -\frac{w}{u}\frac{K_{l-1}(w)}{K_l(w)} \qquad (12)$$

The modal weights of various LP modes at each time can be calculated as [16]:

$$\left| w_{lmi}(t) \right|^2 = \frac{\left| \iint E_{measured}(x,y,t)\, E_{lmi}(x,y)\, dx\, dy \right|^2}{\iint \left| E_{measured}(x,y,t) \right|^2 dx\, dy \iint \left| E_{lmi}(x,y) \right|^2 dx\, dy}. \tag{13}$$

As a result, we can analyze the modal contents and modal weights in the MMF output pulses by fully measuring the spatiotemporal pulse fields using delay-scanned STRIPED FISH.

4. Experimental setup

We performed experiments to demonstrate delay-scanned STRIPED FISH's ability to measure long, complex pulses propagating through MMF. The experimental layout is shown in Fig. 2, starting from a Ti: Sapphire oscillator. Pulses centered at 792nm, with a 25nm FWHM, were spatially filtered by two lenses, L1 and L2 (both of 100mm focal length), and a 75μm diameter pinhole, shaping to a 3-mm-diameter Gaussian profile with relatively flat phase. A beam splitter (BS1) was used to divide 80% of the pulse energy to be used as the test beam and the other 20% for the reference beam. The test beam was given more energy because of the expectation that the MMF would consume a large proportion of the energy as the beam was coupled into it. The test beam was coupled into and collimated out of the MMF (Thorlabs, FG025, 373mm) using objective lenses, L3 (Newport M-60X) and L4 (Newport M-5X) respectively, and a fiber alignment stage with five degrees of freedom, which was used to induce various coupling conditions. If compensation of the MMF's material dispersion was preferred, a single-prism pulse compressor, BOA-8 (Swamp Optics), was inserted to provide the pulse with more negative group delay dispersion (GDD). This served to reduce the pulse's temporal chirp and make the intermodal delay and modal dispersion of the MMF easier to observe. The MMF output served as the unknown pulse, entering the STRIPED FISH apparatus via the beam combiner, BS3. The near-field spatial profile of the MMF output was monitored by a spatial profile camera (PixeLINK PL-A741, 1280 × 1024 pixels, 6.7μm pixel pitch, 8-bit) when a sampler was put in the beam.

While a small percentage of the reference beam was sampled by the beam splitter, BS2, and sent to the GRENOUILLE [19] for characterization, yielding the spectral intensity and phase of the reference pulse, most of the reference beam was transmitted through BS2 to be delayed by a delay stage. The reference pulse was delayed with 167fs delay intervals over the length of the entire unknown pulse and interfered with each specific temporal slice of the MMF output. Finally, the reference and unknown pulses were combined at BS3, passed through a DOE (3μm × 3μm, 15μm spacing photo-masked quartz plate with chrome coatings, rotated ~10°), IBPF (Semrock LL01-852, ~40° tilted, ~5nm bandwidth), two photographic lenses, L5 (Nikon 50mm, f/1.4), L6 (Computar 75mm, f/1.4) and an ANDF (Edmund Optics Apodizing Filter #64-386), and overlapped at the camera (PixeLINK PL-A781, 3000 × 2208 pixels, 3.5μm pixel pitch, 8-bit), where STRIPED FISH traces were captured.
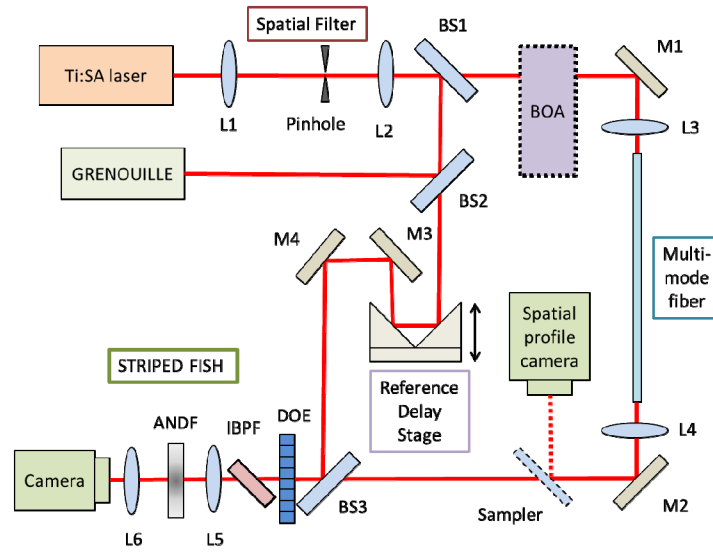
Fig. 2. Experimental layout of delay-scanned STRIPED FISH setup for measuring long output pulses from MMF.

5. Results and discussion

The experimental results show the improvement achieved by delay-scanned STRIPED FISH when dealing with long and complex pulses, compared to single-frame STRIPED FISH. Output pulses with pulse lengths of ~3ps and containing more than ten LP modes from the MMF were generated under different coupling situations and completely characterized using our technique.

Table 1. Cutoff normalized frequency V_c and amplitude profile of first 14 LP modes [24]

LP_{lm} mode	LP_{01}	LP_{11}	LP_{21}	LP_{02}	LP_{31}	LP_{12}	LP_{41}
V_c	0	2.405	3.832	3.832	5.136	5.52	6.38
Mode amplitude profile							
LP_{lm} mode	LP_{22}	LP_{03}	LP_{51}	LP_{32}	LP_{13}	LP_{61}	LP_{42}
V_c	7.016	7.016	7.588	8.417	8.654	8.771	9.761
Mode amplitude profile							

   The numerical aperture (NA) of the 373mm-long MMF used here is 0.1 and its core diameter is 25 μm. When it is used around 792nm, the normalized frequency parameter V is ~9.9, which should support at least 14 LP modes, from LP_{01} to LP_{42} [25]. These LP modes along with their cutoff V numbers and mode amplitude profiles are listed in Table 1. It should also be noted however, that different MMF coupling conditions will change the energy distribution among the supported modes.

5.1 Retrieved intensity and phase of multiple wavelengths at each delay

In the well-centered coupling situation, 20 delay-scanned frames containing STRIPED FISH traces were taken of the MMF output. Figure 3 shows three of those 20 frames which were taken at delays of −1ps, 0ps, and 0.83ps. The wavelengths of the 30 holograms are in ascending order from right to left and from top to bottom between 781nm and 813nm. In these traces, there is a constant background term for each hologram, as shown in Eq. (3), which can be spatially Fourier filtered out during the retrieval process. The fringes vary from frame to frame, recording the complete information of different delayed slices. One should also note that the fringes in the holograms of longer wavelengths (left part of the trace) appeared and disappeared earlier than those in the holograms of shorter wavelengths (right part of the trace). This is because the large material dispersion in MMF makes longer wavelength components travel faster in the fiber than shorter wavelengths. This effect, known as temporal chirp, stretches the pulse to longer than 2ps and beyond the temporal measurement range of single-frame STRIPED FISH.
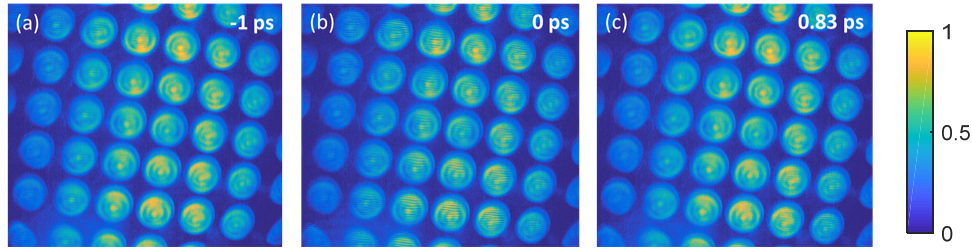
Fig. 3. Three measured delay-scanned STRIPED FISH traces at −1ps, 0ps, and 0.83ps (well-centered coupling). The wavelengths of the 30 holograms are in ascending order from right to left and from top to bottom between 781nm and 813nm. Each hologram occupies 330 × 330 pixels.

In Table 2, we present the retrieved intensity and phase of three wavelengths (784nm, 792nm and 810nm) at four delays (−667fs, −167fs, 167fs and 500fs) in the well-centered coupling situation for discussion. These results were obtained using the retrieval algorithm of $E_{\text{slice}}(x,y,\omega_i;\tau_k)$ derived in section 3.1. The existence of temporal chirp in the MMF output is more obviously observed in the retrieved results by noting that at −667fs the 784nm light has not yet arrived and at 500fs the 810nm light has already passed. In other words, the long-wavelength component is distributed ahead of the short-wavelength counterpart in the long pulse. Furthermore, by comparing the retrieved field of each wavelength at the different delays, we could also notice the effect of intermodal delay: the varying of the spatial profile from a lower-order mode profile to a higher-order mode profile as time elapses, referring to the mode amplitude profiles in Table 1. Taking 792nm as an example, we can see that LP_{11}, LP_{21}, LP_{12} and LP_{03} emerge in time successively, which implies that the different fiber modes propagate with different velocities in the MMF.

After retrieving the intensity and phase of multiple wavelengths at each delay, the entire pulse field $E_{\text{unk}}(x,y,t)$ can be reconstructed by the concatenation method described in section 3.2. A movie revealing the full spatiotemporal information can also be made based on the pulse's spectrogram using the calculation described in section 3.3.

Table 2. The retrieved amplitude and phase of three wavelengths at four delays (well-centered coupling)

Wavelength	784nm		792nm		810nm		Color bars	
Delay	Intensity	Phase	Intensity	Phase	Intensity	Phase	Intensity	Phase
-667fs								
-167fs							1	5
167fs							0.5	0
500fs							0	-5

5.2 Concatenated pulses of different fiber coupling situations

To better analyze the behavior of different fiber modes, the BOA compressor was inserted with an appropriate amount of GDD to compensate for the material dispersion in the MMF. Simultaneous arrival of the fringes at all wavelengths was used as an indication of sufficient GDD compensation. By compensating for the material dispersion, we could highlight the influences of intermodal delay and modal dispersion.

While the material dispersion was compensated, various MMF coupling situations, hence various fiber-mode energy distributions were investigated. The final results of the measured output pulses under four MMF coupling situations are shown in Fig. 4. Figures 4(a)-4(e) represent the well-centered coupling situation. Figures 4(f)-4(j) represent a coupling situation in which there were small offsets from the center in both x- and y-directions. Figures 4(k)-4(o) represent a coupling situation where a small offset in only one direction is used. Figures 4(p)-4(t) represent a large offset coupling situation. To monitor the MMF coupling situations, the spatial profile camera and sampler in Fig. 2 were used to measure the temporally-averaged near-field spatial intensity. The monitored spatial profiles (first column in Fig. 4) offered adequate verification of the accuracy of our measured pulse information. Using the measured complete spatiotemporal pulse fields, the spatially-integrated spectrograms (second column in Fig. 4) were calculated and the reconstructed color movies were made. Three time snapshots from each movie are presented in the last three columns in Fig. 4. These snapshots correspond to the three different time points marked with dashed or dotted lines in each spectrogram. The intensity of every snapshot shown here was set to the same level to display more fiber mode details, yet the intensity in the color movies remained unchanged, demonstrating the spatiotemporal intensity distribution of the actual pulses. The color movies can be found in their entirety in the supplementary materials of this paper. Since the STRIPED FISH apparatus was placed in the far field position, the measured profiles contain the far-field features of the fiber modes, where the radii of higher modes are larger than those of lower modes. This is affirmed by the size change among the three snapshot columns in Fig. 4.
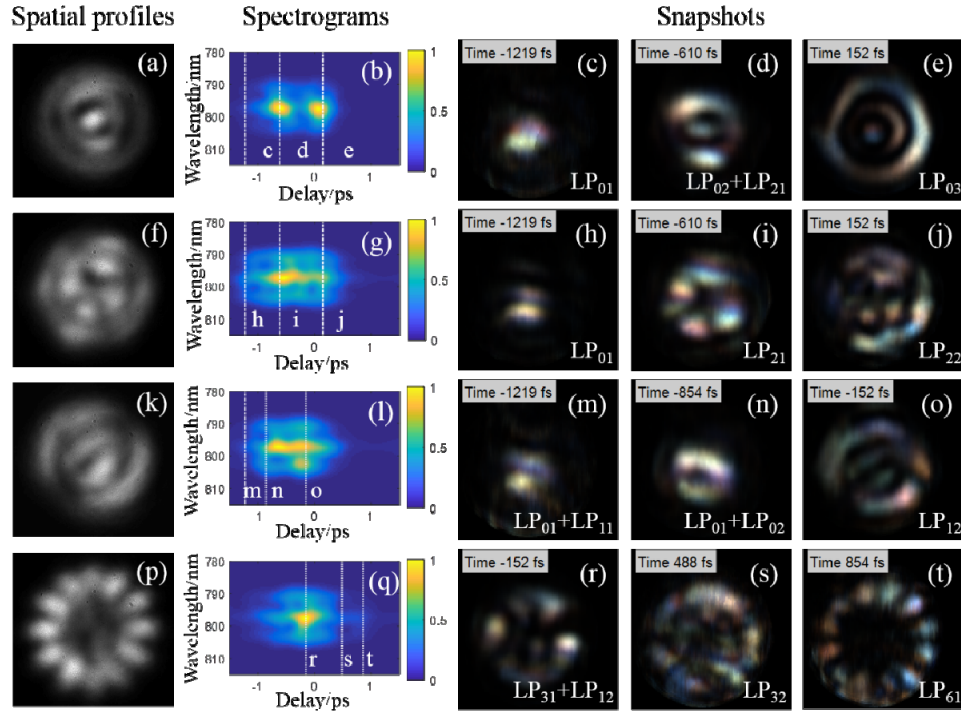
Fig. 4. Measured results of MMF output pulses of different fiber coupling situations. Centered coupling situation: (a) near-field spatial profile; (b) calculated spectrogram; (c-e) three selected time snapshots from the reconstructed color movie (see Visualization 1); Small offsets in both x- and y-direction situation: (f) near-field spatial profile; (g) calculated spectrogram; (h-j) three selected time snapshots from the reconstructed color movie (see Visualization 2); Small offset in only x-direction situation: (k) near-field spatial profile; (l) calculated spectrogram; (m-o) three selected time snapshots from the reconstructed color movie (see Visualization 3); Large offset situation: (p) near-field spatial profile; (q) calculated spectrogram; (r-t) three selected time snapshots from the reconstructed color movie (see Visualization 4). Spectrograms in the second column are spatially integrated and showing overall spectro-temporal energy distribution and dispersion of the existing fiber modes. The labeled dashed and dotted lines in the spectrograms are in accordance with the label of the time snapshots. The snapshots show the spatial intensities (by brightness) and frequencies present (by color) at different times. Every snapshot has one or two dominant LP modes, which are labelled in the snapshots. Temporal sums of these snapshots of these four situations agree with the monitored near-field spatial profile well, providing validity to delay-scanned STRIPED FISH.

In the well-centered situation, the pulse appeared at -1219fs with an LP_{01} mode shape in space (Fig. 4(b) dashed line c and Fig. 4(c)) and lasted ~2ps in time. Most of the pulse energy was localized in time around -610fs (dashed line d) and 152fs (dashed line e). While the snapshot at 152fs in Fig. 4(e) reveals the existence of an LP_{03} mode, the snapshot at -610fs in Fig. 4(d) shows a combined intensity of LP_{01} and LP_{11} modes overlapped with each other in time, which was analyzed with the modal decomposition method described in section 3.4. The superposition of the dominant modes in these snapshots agreed well with the monitored near-field spatial profile in Fig. 4(a).

When small offsets from the well-centered coupling were introduced in both x- and y-directions, the near-field profile changed to Fig. 4(f). The three snapshots in Figs. 4(h)-4(j), share the same time positions as the centered-coupling case. Due to the change in coupling however, the energy distribution in time and the generated modes differed significantly. From the spectrogram in Fig. 4(g), the energy was observed to spread more between -610fs and 152fs (dashed lines i and j). Still, the mode at -1219fs was mainly LP_{01}, as shown in Fig.

4(h), because the intermodal delay of the fiber remained the same, which means that no matter what coupling situation, the appearance time and vanishing time of each mode did not change. However, the coupling did affect which modes were excited and how much energy each mode in the pulse received. A comparison between Figs. 4(i) and 4(d) suggests that when coupling with small 2D offset, the LP_{21} mode now receives more energy than the LP_{11} mode (which had previously dominated at −610fs in the well centered coupling situation) while the LP_{31} mode is also excited. By comparing Figs. 4(j) and 4(e), the 152fs time frame is seen to be dominated by the LP_{22} mode in the small offset situation instead of LP_{03} as in the well-centered situation. This exchange of energy between LP_{22} and LP_{03} is possible because both modes have the same cutoff normalized frequency and thus show up at the same time.

In the case of small offset coupling in only one direction (x), the modal decomposition analysis revealed at −1219fs that while the LP_{11} mode did receive more energy at this time, the LP_{01} mode still dominated the profile shape, see Fig. 4(m). At −854fs, an interesting singular optical vortex profile was formed by a composition of multiple modes, see Fig. 4(n). Then at −152fs the LP_{12} mode overwhelmed the others in the pulse spatial profile, see Fig. 4(o).

In contrast, in the large offset coupling situation shown in Figs. 4(p)-4(t), more energy was coupled into higher order modes and more modes were excited, such as LP_{21}, LP_{31}, and LP_{41} at −152fs in Fig. 4(r), LP_{32} at 488fs in Fig. 4(s) and LP_{61} at 854fs in Fig. 4(t). The pulse was elongated to ~3ps in the large offset coupling situation because the higher modes appeared at larger delays, which can be intuitively seen from the spectrogram in Fig. 4(q). Under all three offset coupling situations, the sum of far-field snapshots matched the mode contents of the near-field spatial profiles well.

The spectrograms exhibited the overall spectro-temporal energy distribution and dispersion of the existing fiber modes. Comparing the column of spectrograms in Fig. 4, center-coupling modes were un-chirped due to the sufficient compensation of material dispersion (GDD) by the BOA compressor and well separated because of the intermodal delay, as shown in Fig. 4(b). The modal dispersion acted to broaden each mode to ~200fs duration, however. When coupling was offset as in Figs. 4(g) and 4(l), more fiber modes were excited and received pulse energy. As more coupling offset was introduced, as in Fig. 4(q), lower fiber modes received less energy while more energy was distributed into higher modes.

Although the snapshots resembled one-mode or two-mode-overlap shapes, there were many more modes present at the same time according to the modal decomposition results. Their energy ratios varied so greatly that some of them could not be seen from the average intensity profile. Their influence however, was captured well by the phase information which was expressed by the color variations between the snapshots.
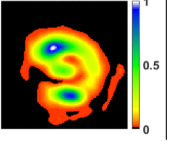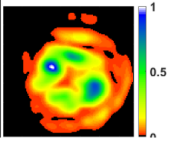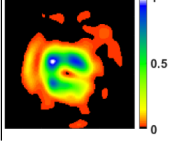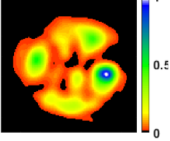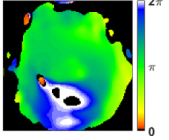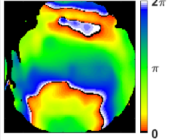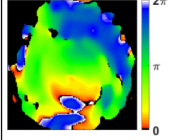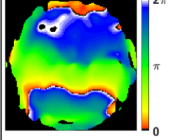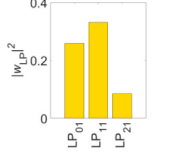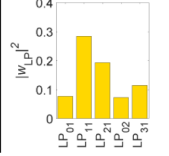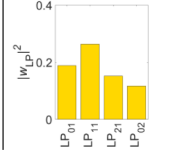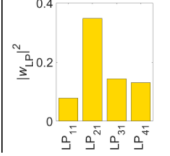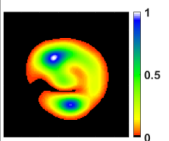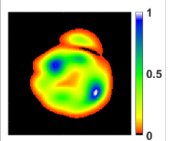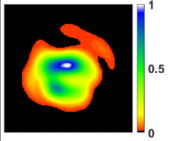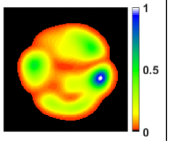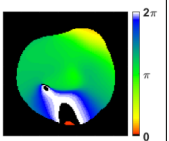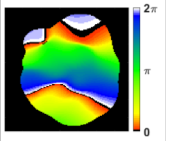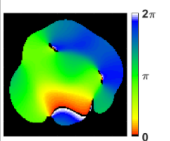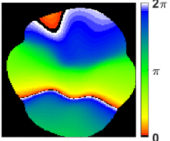
5.3 Modal decomposition analysis of the concatenated pulses

Modal decomposition is a powerful tool to understand fiber modes when more than one mode exists at the same time. A sample of the snapshot decomposition results of the concatenated pulses are shown in Table 3. The decomposition results tell us which modes are generated and how much weight in energy they have at a certain time. The pulse field at each time can then be composited according to the decomposition results.

Based on the decomposition analysis, the overall mode weights of the complex spatiotemporal pulses from the multi-mode fiber under the four coupling situations were calculated. Figure 5(a) is the centered coupling situation; Fig. 5(b) is the small offsets in both x- and y-direction situation; Fig. 5(c) is the small offset in only x-direction situation; Fig. 5(d) is the large offset situation.

Table 3. The decomposition results of the measured snapshots

Coupling and time	Centered −610fs	Small x and y-offsets −610fs	Small x-offset −854fs	Large offset −152fs
Measured intensity				
Measured phase				
Decomposition result				
Intensity fitted to mode-weights				
Phase fitted to mode-weights				

STRIPED FISH is a technique based on the principles of interference, meaning that the interference fringes present in STRIPED FISH's traces only occur when the two beams, the unknown and reference beams, have the same polarization. Thus, since the reference pulse used in this experiment has p-polarization, the information obtained will also only correspond to the similarly polarized component of the unknown pulse. With this being said, the MMF used in our experiment was not designed to maintain the unknown pulse's original p-polarization and changed portions of the beam's energy from p-polarization to s-polarization, for example. However, in many of the cases observed, we estimate that a significant majority of the beams' original polarization was maintained. This conclusion is evidenced by our ability to still achieve agreement between the corresponding measured and fitted intensities in Table 3.

In addition to possible polarization loss, imperfections in the fiber such as elliptic deformation and micro-bending may also have caused complex mode couplings to occur [26]. As a result, a few of the constructed fields could not be fitted to the LP modes properly. While a similar delay-scanned STRIPED FISH measurement of the other polarizations present would alleviate issues associated with polarization loss, an ability to identify possible mode couplings can be useful for fiber imperfection detection and constructing higher quality fibers [27].
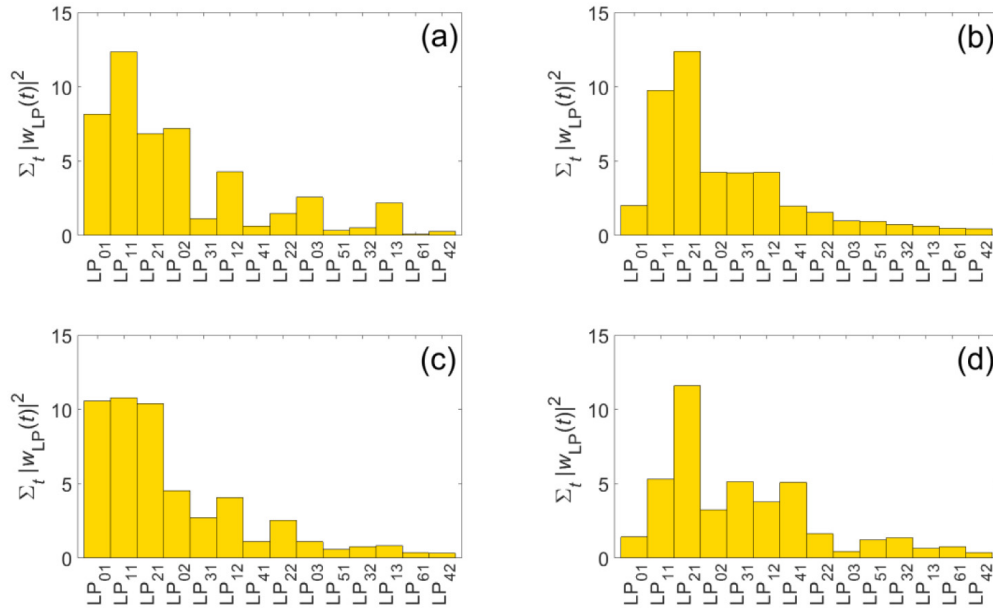
Fig. 5. Decomposition analysis of the concatenated pulses. (a) centered coupling situation; (b) small offsets in both x- and y-direction situation; (c) small offset in only x-direction situation; (d) large offset situation.

6. Limitations of delay-scanned STRIPED FISH

While not limited by the bandpass filter, the temporal range and spectral resolution of delay-scanned STRIPED FISH have a new, albeit less stringent, limitation, which is provided by the dynamic range of the camera. When the unknown pulse becomes longer and the reference pulse remains unchanged, the reference pulse only forms spatial interference fringes with the temporal component of the unknown pulse with which it temporally overlaps. The rest of the unknown pulse simply provides an approximately constant background underneath each hologram. The longer the unknown pulse, the more constant background there will be in every hologram. Meanwhile, the informative fringes remain at the same intensity level. In other words, the visibility of the fringes decreases as the unknown pulse increases in length, and more delay is required. This reduction in fringe visibility at large delays reduces the effective dynamic range of the camera for informative fringes and experimentally limits the maximum length of unknown pulse. An 8-bit camera can distinguish the fringes with a visibility as low as 0.0078 and a 10-bit camera can use a value as low as 0.002. Thus, for such cameras, the unknown pulse can be 128 and 512 times longer than reference pulse, respectively. Therefore, using an 8-bit (10-bit) camera, delay-scanned STRIPED FISH can measure pulses of $128\Delta T_{\text{SF}}$ ($512\Delta T_{\text{SF}}$) length, which is much larger than the time range of single-frame STRIPED FISH. Furthermore, a camera with deeper dynamic range could extend the delay-scanned STRIPED FISH's time range to even longer values.

In this work, we used an inexpensive 8-bit camera and 3nm-bandwidth filter to measure ~3ps complex pulses from MMF with delay-scanned STRIPED FISH. According to the

previous discussion, this delay-scanned STRIPED FISH is capable of measuring much longer pulses (~nanoseconds). However, because we chose to use a simple prism pulse compressor to compensate for the material dispersion of MMF, the ~-15,000fs^2 of negative dispersion available from it set the limit for the longest length of MMF we could test. Under this limitation, we used a 373mm-long MMF, and the pulses from such MMF are ~3ps long. Given that the single-frame STRIPED FISH with the same camera and filter can only measure pulses up to ~300fs (a few ps with a very expensive narrower-band filter), the 3ps-temporal-range demonstration presented here should serve as a sufficient indication of delay-scanned STRIPED FISH's improved ability to measure much longer pulses from longer fibers.

7. Conclusion

In summary, we have introduced a delay-scanned STRIPED FISH technique capable of spatiotemporally measuring the full intensity and phase information of long, complex pulses. Using this technique, we have extended the temporal range of STRIPED FISH by a factor of ten and characterized ~3ps long MMF output pulses containing more than ten fiber modes. The material dispersion of the test fiber was diagnosed in the retrieved data and pre-compensated allowing the intermodal delay and modal dispersion of ten fiber modes from LP_{01} to LP_{42} to be intuitively observed from the reconstructed spatiotemporal movies. Good agreement between the reconstructed pulse movies and the monitored near-field spatial profiles were used to demonstrate this technique.
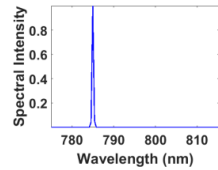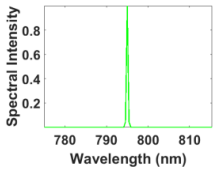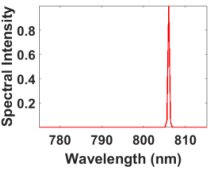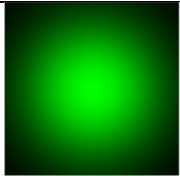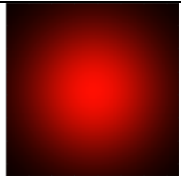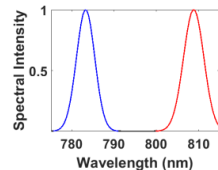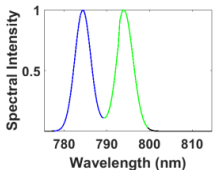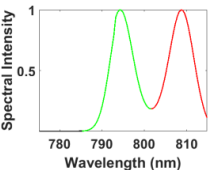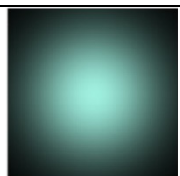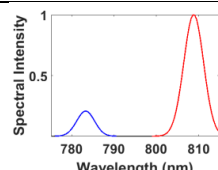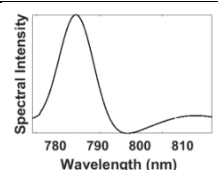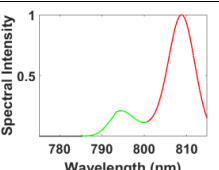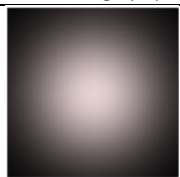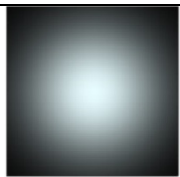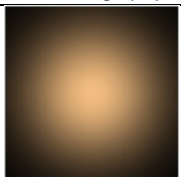
The capabilities of the measurement, temporal length, and number of modes are no longer limited by the narrower bandpass filter. Theoretically, delay-scanned STRIPED FISH can measure any spatiotemporally complex pulse within its spatial and temporal resolutions. In practice, the number of fiber modes that can be observed depends on the energy proportion of the modes, the sensitivity of the camera, and the number of pixels of the camera. And the maximum measurable pulse length is limited by camera's dynamic range. In other words, longer and more complex pulses with more fiber modes can be measured using a camera with higher sensitivity and deeper dynamic range.

We believe this simple and inexpensive technique can be used in not only MMF output pulse characterization as demonstrated in this paper, but also in many other interesting applications associated with long and spatiotemporally complex pulses.

Appendix

As discussed in section 3.3, the color scheme that was used to generate the movies in the Visualization 1 to Visualization 4 is represented in Table 4.

Table 4. The color scheme used for the Visualizations

Funding